

Journal of Materials Chemistry A

Accepted Manuscript



This is an *Accepted Manuscript*, which has been through the Royal Society of Chemistry peer review process and has been accepted for publication.

Accepted Manuscripts are published online shortly after acceptance, before technical editing, formatting and proof reading. Using this free service, authors can make their results available to the community, in citable form, before we publish the edited article. We will replace this *Accepted Manuscript* with the edited and formatted *Advance Article* as soon as it is available.

You can find more information about *Accepted Manuscripts* in the [Information for Authors](#).

Please note that technical editing may introduce minor changes to the text and/or graphics, which may alter content. The journal's standard [Terms & Conditions](#) and the [Ethical guidelines](#) still apply. In no event shall the Royal Society of Chemistry be held responsible for any errors or omissions in this *Accepted Manuscript* or any consequences arising from the use of any information it contains.

ARTICLE

Fast and Low Temperature Growth of Electron Transport Layer for Efficient Perovskite Solar Cells

Cite this: DOI: 10.1039/x0xx00000x

Jie Zhang^a, Emilio José Juárez-Pérez^b, Iván Mora-Seró^b, Bruno Viana^a and Thierry Pauporté^{a,*}Received 00th January 2012,
Accepted 00th January 2012

DOI: 10.1039/x0xx00000x

www.rsc.org/

We describe a fast, simple and low temperature electrochemical technique for the preparation of zinc oxide layers on rigid and flexible substrates. The layers, prepared from zinc nitrate precursor, are of high structural and optical quality. They have been optimized to be applied as efficient electron transport layers in CH₃NH₃PbI₃-sensitized perovskite solar cells (PSC). We show that an electrodeposition time of only two minutes and a low processing temperature are sufficient to fabricate solar cells with a power conversion efficiency close to 11%, with a high short circuit current and a small J-V curve hysteresis. The key parameters of the cell functioning have been analyzed over a large applied voltage range by the impedance spectroscopy technique. The solar cell characteristic changes with the ZnO layer deposition time are explained by the variation of the recombination and the charge transfer resistances.

1. Introduction

Solution-processed organic and hybrid organic–inorganic solar cells have been intensely developed during the last two decades.^{1–3} Very recently, perovskite solar cells (PSC) have emerged as the most promising new generation of hybrid photovoltaic devices.^{4–13} The power conversion efficiency of this newcomer has raised fast and very recently a certified power conversion efficiencies (PCE) higher than 20% has been reported.¹⁴ The most extended perovskite materials used for the solar light absorption and charge generation are hybrid organic–inorganic compounds with a 3D crystal structure of general formula CH₃NH₃PbX₃ (with X=Cl, Br or I). The electron and hole charge collection is ensured by the two adjacent selective contact phases that generate the driving force for the charge separation. The electrons are usually selectively collected by a wide bandgap oxide material, also called the electron transport layer (ETL), while holes are selectively transferred to a hole transport layer (HTL), usually made of an organic molecular glass. Spiro-OMeTAD is the most common material employed for this purpose.

Currently, most state-of-the art PSCs utilize mesoporous TiO₂ scaffold layers on top of a compact titania layer to provide a substrate on which the perovskite can be grown.⁷ The preparation of these layers requires annealing and sintering processes at high temperature, typically 500°C. On the other hand, other wide bandgap oxides and low temperature processing of the ETL are much less-documented. The low

temperature and fast processing are desirable to reduce the production cost and for the preparation of flexible lightweight devices on plastic substrates. ZnO is a wide bandgap semiconductor with electron affinity similar to TiO₂. It can be grown by various techniques with a high structural quality at low temperature.^{15,16} It is therefore a very promising candidate for the PSC application.^{17–24} Moreover, the conductivity of ZnO is several orders of magnitude higher than the TiO₂ one and that favors the electron transport toward the back contact.^{25,26} Kelly et al.²¹ have recently reported remarkably high efficiency PSCs using a thin layer of dense planar ZnO prepared by spin-coating. The review of the literature on ZnO-PSCs also indicates that remarkably high J_{sc} can be achieved with ZnO ETM.^{17,20}

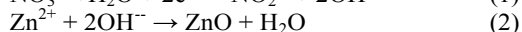
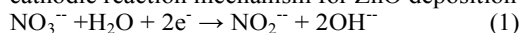
The present work focuses on the preparation by electrochemical deposition of ZnO layers with tailored properties. The advantages of the technique include the deposition at low temperature of high quality material, the precise control of the (nano)structure morphology and thickness, the control of the electrical properties and the excellent electrical contact between the deposited layers and the substrate.^{27–29} Hereafter, we describe the fast and low temperature electrochemical growth of fully-covering ZnO layers using zinc nitrate as the deposition precursor. We show that the deposited material is ZnO of high optical and structural quality. The interest of this layer use as an ETL is demonstrated. After sensitization by CH₃NH₃PbI₃ and cell completion, we have found that the optimized ETL deposition time is very short, only 2 minutes. These

characteristics make this method extremely interesting since TiO₂ alternative for ETL requires much more time and temperature for an optimized efficiency.^{4,5,7} PSCs based on this electrodeposited ZnO layer achieved a PCE of 10.6% with a low J-V curve hysteresis.

2. Experimental

2.1. ZnO layer electrodeposition.

The ZnO films were prepared directly on ITO coated glass substrates. The substrates were carefully cleaned with soap, rinsed with deionized water prior to be sonicated 5 min in ethanol and 5 min in acetone. The electrochemical depositions were carried out in a three-electrode cell. The counter-electrode was a zinc wire and the reference electrode was a saturated calomel electrode (SCE) (with a potential at +0.25V vs NHE) placed in a separate compartment maintained at room temperature. To ensure a deposition as homogeneous as possible, the substrate was fixed and contacted to a rotating electrode and the deposition was performed at a constant rotation speed of 145 rotations per minute (rpm). The deposition bath was a solution of Zn(NO₃)₂ at a concentration of 0.08M dissolved in MilliQ quality water (18.2 MΩ.cm) maintained at 60°C.^{30,31} The deposition was performed at a constant applied voltage of -1.15 V/SCE for various times. The cathodic reaction mechanism for ZnO deposition is:^{28,29}



2.2. Solar cell preparation and characterizations.

The ZnO layers were dried at 150°C for 1h. The organic-inorganic perovskite CH₃NH₃PbI₃ was deposited by a sequential method inspired from the literature.⁶ 70 μL of PbI₂ solution at 70°C (dissolved in N,N-dimethylformamide at a concentration of 460 mg.mL⁻¹) was spin-coated on top of the ZnO layer at 3,000 rpm. for 15 s. This step was repeated once. After drying at 70°C for 30 minutes in air, the substrate was dipped into a solution of CH₃NH₃I in 2-propanol (10 mg.mL⁻¹) for 30 s (optimized duration), then dried at 70°C for 30 min. CH₃NH₃I was prepared according to Ref.³². Subsequently, the spiro-OMeTAD-based hole-transport layer was deposited using a solution containing 80 mg spiro-OMeTAD, 28.5 μL 4-tertbutylpyridine and 17.5 μL of lithium-bis(trifluoromethanesulfonyl)imide (Li-TFSI) (520 mg Li-TFSI in 1 mL acetonitrile) all dissolved in 1 ml chlorobenzene. This precursor solution was deposited by spin coating at 2,000 rpm for 15 s. Finally, a 100-nm-thick silver layer was deposited by thermal evaporation on the Spiro-OMeTAD layer as a back contact.

The J-V curves were recorded by a Keithley 2400 digital sourcemeter, using a 0.15 V.s⁻¹ voltage sweep rate, for which the measured curve hysteresis was low. The solar cells were illuminated with a solar simulator (Abet Technology Sun 2000) filtered to mimic AM 1.5G conditions. The illuminated surface was delimited by a black mask with an aperture diameter of 3

mm. The power density was calibrated to 100 mW.cm⁻² by the use of a reference silicon solar cell. The reproducibility of the performances was checked on several cells prepared from different batches. The impedance spectra were measured under 0.95-1 sun illumination provided by a Schott lamp, between 600 KHz and 0.12 Hz, using a Solartron FRA1255 frequency response analyzer coupled with a PAR273 EGG potentiostat. The AC signal was 20 mV.

The film thicknesses were measured with a Dektak 6M stylus profilometer. The sample morphologies were examined with a high resolution Ultra 55 Zeiss FEG scanning electron microscope (FE-SEM) at an acceleration voltage of 10 kV. The film structure was characterized by a Phillips X-Pert high-resolution X-ray diffractometer (XRD) operated at 40 kV and 45 mA and using the CuKα radiation with λ = 1.54056 Å. The film total transmissions and total reflections were measured with a Cary 5000 UV-Vis-NIR spectrophotometer equipped with an integrating sphere. The absorbance spectra were calculated from these two parameters. The photoluminescence measurement system combined a YAG:Nd laser and a HR250 monochromator (Jobin-Yvon) coupled to a UV-enhanced intensified charge-coupled device (ICCD; Roper). The excitation wavelength was 266 nm for ZnO and 600 nm for perovskite characterizations. Raman scattering measurement was performed at room temperature with a Renishaw INVIA apparatus equipped with a microscope and a CCD detector. A 532 nm solid-state green laser was used for off-resonance excitation with 50mW power. The instrument was calibrated using a silicon standard.

3. Results and discussion

The oxide layers for electron transport were grown on ITO/glass substrate by electrodeposition using 0.08M Zn(NO₃)₂ as the zinc and hydroxide precursor with an applied potential of -1.15V vs SCE (saturated calomel electrode) and a temperature of 60°C. The technique generate n-type doped ZnO layer that are hereafter noted i-ZnO. The Fig.1 is the variation of the deposition current due to nitrate reduction reaction on the ITO electrode surface. The cathodic current rapidly decreased before to stabilize at the low value of -0.35 mA.cm⁻² and then leveled off after 20s of deposition time (t_d). After 100s, the deposition current reached a plateau at -9.5 mA.cm⁻². The curve shape is similar to that observed for the electrodeposition of ZnO at room temperature using a chloride medium.³³ It is explained by the progressive nucleation of ZnO on the ITO surface. We show below that more than 100s is necessary to fully cover the electrode surface. The electrical charge exchanged during the deposition of the investigated layers (corresponding to 20s, 50s, 120s and 300s of t_d) are plotted in Fig.1. From this parameter, we have calculated the equivalent ZnO layer thickness deposited onto the electrode for various electrodeposition times. The values are gathered in Table 1 and are compared to the actual layer thicknesses measured by profilometry. The latter are significantly higher than the calculated ones with a gap between the two values which decreases with time. We also observed that the roughness increased with the t_d (Table 1).

Table 1 Effect of i-ZnO deposition time on the layer characteristics after annealing at 150°C for 1h.

Deposition time/ s	$Q^a / C.cm^{-2}$	Calculated thickness ^b / nm	Measured thickness/ nm	R_q^c / nm	λ_{UV}^d / eV (nm)	E_g^e / eV
20	0.031	23	X	X	X	X
50	0.170	128	250	18	3.26 (380)	3.40
120	0.645	485	780	65	3.23 (384)	3.38
300	2.005	1510	1900	120	3.22 (385)	3.32

^a Q , the electrical charge density exchanged during the electrodeposition process.

^b Obtained from the measured total electrical charge exchanged, see Fig.1, as :

$D(\mu m) = \frac{Q}{nF} \frac{MW}{\rho} = 0.7519 Q(C.cm^{-2})$, with n the number of electrons exchanged in the electrochemical reaction (1)-(2) ($n=2$), F the Faraday constant ($96\,485\ C.mol^{-1}$), MW the molar weight of ZnO ($81.4\ g.mol^{-1}$) and ρ the density of ZnO ($5.61\ g.cm^{-3}$).

^c Root mean square of roughness (RMS)

^d Near-Band edge UV photoemission energy (wavelength).

^e Measured from the transmittance and reflectance spectra.

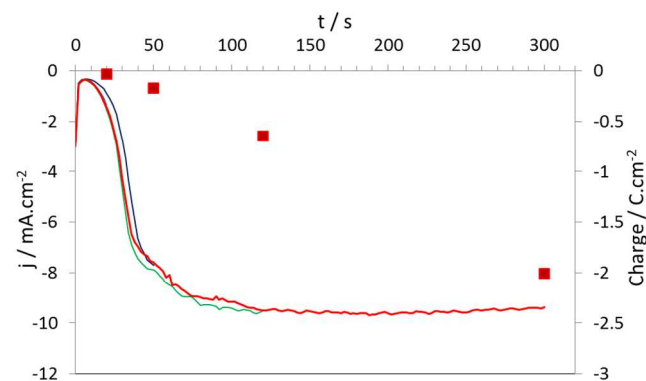


Fig. 1 Variation of the current density (lines) and electrical charge exchanged (red dots) with deposition time ($E = -1.15\ V/SCE$, $T = 60^\circ C$). Three deposition curves for different deposition times are presented in blue (50s), green (120s) and red (300s).

Scanning electron microscopy (SEM) images of the layers are shown in Fig. 2a-d. After 20s, the deposit is made of grains dispersed on the ITO surface (Fig. S1, Supplementary information). After 50s the substrate is not fully covered and in Fig. 2a the arrows point out the bare ITO substrate zones uncovered by the deposit. However, after 120s, a layer made of large grains that perfectly covers the ITO substrate is observed (Fig. 2b-c). On the cross-sectional view of Fig. 2d, some prominent ZnO grains emerge from the layer that explain the roughness observed by profilometry. The close inspection of the grain surface shows no crystal facets but ten-nanometer-sized asperities (Fig. 2c). Moreover the cross-sectional view (Fig. 2d) exhibits the presence of pinholes in the grains. These voids suggest some porosity of the layers that explains in part the underestimation of the calculated layer thicknesses compared to the measured ones in Table 1.

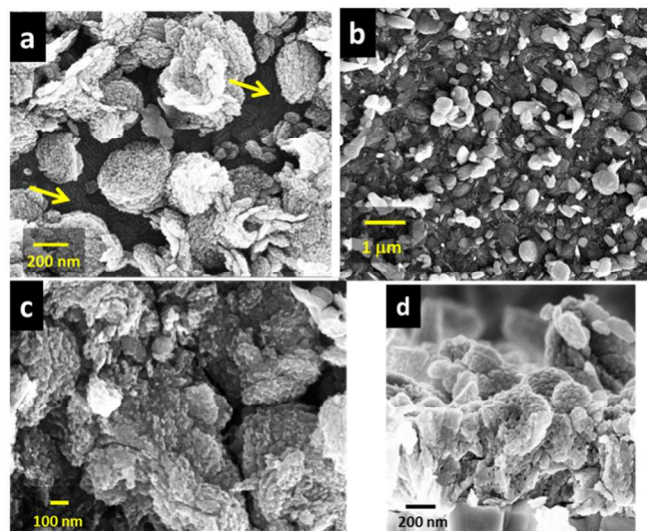


Fig. 2 FE-SEM images of (a) i-ZnO layer deposited on ITO for 50s, (b-d) i-ZnO layer deposited on ITO for 120s (b,c) top views, (d) cross-sectional view.

The i-ZnO layers have been characterized after an annealing treatment in air at 150°C for 1h. The XRD measurements are presented in Fig. 3a. For 20s of t_d no ZnO was detected. After 50s, the (101) ZnO reflection peaks could be observed and for longer deposition times the main diffraction peaks were assigned to the hexagonal wurtzite structure of ZnO. The comparison of the relative intensity of the peaks with the JCPDS 036-145134 reference card³⁴ shows that there was no special texturation of the layer. The layer Raman spectra are presented in Fig. S2a (Supplementary Information). The optical phonons at the G point of the Brillouin zone belong to the representation: $\Gamma_{opt} = A_1(z) + 2B_1 + E_1(x,y) + 2E_2$ where x , y , z represent the polarization directions. A_1 and E_1 modes are polar and split into TO-transverse optical and LO-longitudinal optical components.³⁵ The E_2 modes are Raman active only.

The B_1 modes are infrared and Raman inactive or silent modes. The dominant emission peaks at 100 cm^{-1} and 438 cm^{-1} , are attributed to the low- E_2 and high- E_2 modes of non-polar optical phonons, respectively. The broad peak at about 331 cm^{-1} , seen in the spectrum of i-ZnO(300s) is attributed to a $E_2^H-E_2^L$ (multiphonon) mode.^{36,37} The sharpness and high intensity of the E_2 -mode emissions confirm the well-crystallization of the wurtzite ZnO films beyond two minutes of deposition time.

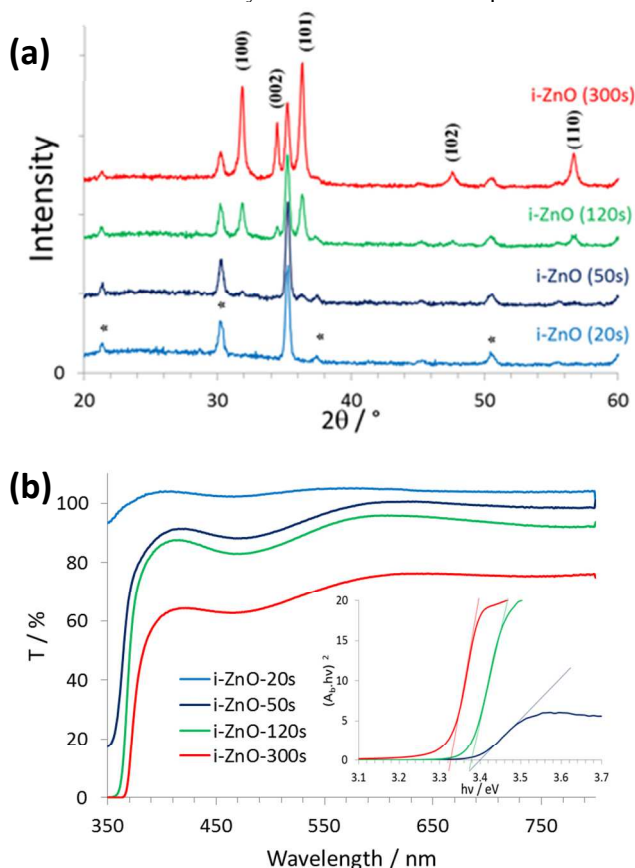


Fig. 3 (a) XRD patterns of i-ZnO layers (the ITO substrate reflections are marked with stars). (b) Total optical transmittance of the i-ZnO layer for various deposition times. The inset is the direct bandgap determination.

The layer optical properties are presented in the Fig. 3b. The i-ZnO(20s) transmission curve exhibits a very small UV-edge due to its thinness and no-covering nature. For i-ZnO(50s) the low wavelength transmission is not zero because the ZnO electrodeposited layer do not fully cover the ITO substrate. From the absorption edge at about 370 nm , the ZnO bandgap (E_g) has been calculated for the various layers (see inset in Fig. 3b) and the values are gathered in the Table 1. They slightly decreased with the deposition time. The room temperature photoluminescence is shown in Fig. S2b (Supplementary information). The spectra are characterized by a strong near-band-edge UV emission which increases in intensity with the deposition time and then with the layer thickness. There is also a weak green emission centered at 530 nm due to intrinsic defects. The intensity ratio between the UV emission and the visible one clearly increases with t_d . It is the signature of an improvement of the layer structural quality with this parameter. The wavelengths of the UV emission, reported in the Table 1, slightly shift towards a lower energy with the oxide deposition

time maybe because of a reduction of the hydroxide content in the deposit.

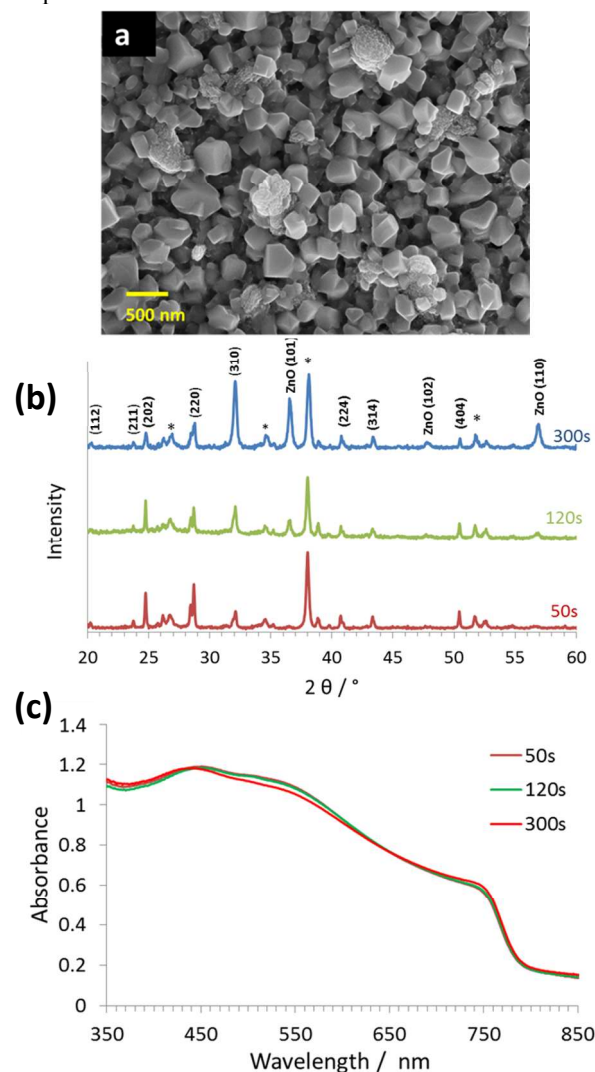


Fig. 4 (a) FE-SEM top view of a i-ZnO(120s) layer sensitized with $\text{CH}_3\text{NH}_3\text{PbI}_3$. (b) XRD patterns (the ITO substrate reflections are marked with stars) and (c) absorbance of i-ZnO/ $\text{CH}_3\text{NH}_3\text{PbI}_3$ layers.

The i-ZnO layers have been sensitized by the $\text{CH}_3\text{NH}_3\text{PbI}_3$ hybrid perovskite using a two-step technique described in the experimental section.⁶ The perovskite deposition process resulted in the covering of the i-ZnO surface by grains with a mean size of about 300 nm (Fig. 4a). The XRD patterns, shown in Fig. 4b, are characteristics of well-crystallized $\text{CH}_3\text{NH}_3\text{PbI}_3$ whatever the i-ZnO deposition time used. The mean reflection peaks are indexed in Fig. 4b. The absorbance spectra are shown in Fig. 4c. The lead iodide perovskite layers deposited on ZnO scaffolds show a panchromatic absorption of light with spectra that extend from near-UV to near infra-red regions. The absorbance intensity does not depend on the i-ZnO deposition time and then on the roughness of the initial i-ZnO layer. The band edge analysis shows that the prepared $\text{CH}_3\text{NH}_3\text{PbI}_3$ has a direct bandgap of 1.58 eV (Fig.S3a, Supplementary information). The high structural quality of the perovskite layers has been confirmed by the photoluminescence measurements at room temperature with a strong emission peak centered at 777 nm (Fig.S3b, Supplementary Information).

ARTICLE

Table 2 Effect of the i-ZnO layer deposition time on the J-V curve characteristics (AM1.5G filtered full 1 sun illumination, FF is the curve fill factor).

i-ZnO deposition time/s	Scan direction ^a	V_{oc} / V	J_{sc} / mA.cm ⁻²	FF/ %	PCE/ %
20	SC-FB	0.41	11.2	20.59	0.94
	FB-SC	0.29	5.43	25.11	0.39
50	SC-FB	0.89	20.1	37.2	6.68
	FB-SC	0.87	18.9	45.5	7.51
120	SC-FB	0.89	23.1	50.0	10.25
	FB-SC	0.91	22.6	52.9	10.91
300	SC-FB	0.81	21.8	54.07	9.56
	FB-SC	0.84	21.8	54.02	9.89

^a SC-FB : Short circuit to forward bias. FB-SC: Forward bias to short circuit.

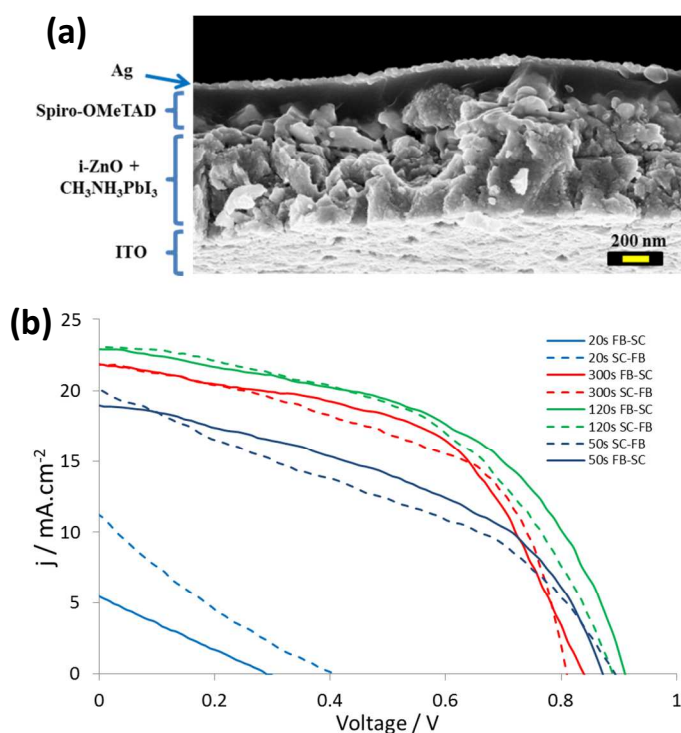


Fig. 5 (a) FE-SEM cross-sectional view of ITO/i-ZnO/CH₃NH₃PbI₃/Ag cell. (b) Effect of i-ZnO deposition time on the J-V curves. (100 mW.cm⁻² AM1.5G filtered illumination). Full line FB-SC, dashed line SC-FB scanning directions. Pale blue: i-ZnO(20s); Blue: i-ZnO(50s); Green: i-ZnO(120s); Red: i-ZnO(300s).

The sensitized i-ZnO structures were completed by spin-coating a thin HTL of Spiro-OMeTAD. Finally, a silver contact was evaporated on the top of the HTL. Fig.5a is a SEM cross-sectional view of the multilayer stacking in the case of a i-ZnO(120s) cell. The cell performances have been evaluated by recording the current-voltage curves under calibrated 1 sun

illumination. In Fig.5b, we present the curves measured in the short-circuit (SC) to forward bias (FB) and in the FB to SC scanning directions to give the account of the J-V curve hysteresis.³⁸ The photovoltaic parameters of typical cells are tabulated in Table 2 for the two scan directions. The cells prepared with i-ZnO(20s) had a very low efficiency with a low V_{oc} , FF and J_{sc} because the oxide selective contact was almost absent in that case. It resulted in the direct contact of the perovskite with the ITO substrate layer and the cell was not stable. The i-ZnO(50s) cell exhibited higher J_{sc} , V_{oc} and FF. The best PCE was achieved for i-ZnO(120s) devices. In that case the J_{sc} was high (~23 mA.cm⁻²). Taking the actual cell PCE as the mean value for the two scan directions,³⁸ we found an actual PCE value of 10.6%. Increasing the i-ZnO deposition time was detrimental for the cell performances. In that case the FF slightly increased, but the cell V_{oc} and J_{sc} were reduced compared to i-ZnO(120s). The slight photocurrent reduction for i-ZnO(300s) cannot be assigned to a reduced light harvesting efficiency since the active layer absorbance do not vary significantly with the i-ZnO deposition time (Fig. 4c). The IPCE curves (Fig.S4, Supplementary information) suggest that the charge injection/collection is slightly reduced in i-ZnO(300s) giving rise to a slightly lower J_{sc} .

In order to understand the variation in the V_{oc} and FF between the most efficient devices, impedance spectroscopy (IS) measurements have been performed under illumination over a large applied voltage and frequency range. We have focused on stable cells, i-ZnO(120s) and i-ZnO(300s), where the ZnO covering of ITO is complete. Those with shorter i-ZnO layer deposition times were not stable under a prolonged polarization at various voltages, as required for an adequate IS analysis. The obtained IS spectra only contains a couple of arcs (Fig.6a). These spectra can be fitted using the simple equivalent electrical circuit shown in Fig.6b.²⁰ R_s is the contact resistance due to wiring and ITO layer measured at high frequency. The high frequency arc is ascribed to the parallel association of R_{sc} , a resistance dominated by the selective contact (sc) in parallel with C_{sc} , which is an interfacial capacitance. R_{sc} resistance is influenced by transport resistance at the ETL and HTL, but also

by the charge transfer resistance at the sc-perovskite interfaces.²⁰ In most of the cases, current between two different materials experience a resistive effect when charge moves from one material into the other, originating a charge transfer resistance at the interface. This interfacial resistance decreases as interfacial area increases as resistivity is inversely proportional to the area. In the analyzed case, as perovskite/HTL does not change, the observed differences can be attributed to the perovskite/ZnO interface. At low frequency, another arc is found originated by the parallel association of R_{rec} , the recombination resistance, in parallel with a dielectric relaxation capacitance³⁹ (modelled by a constant phase element (CPE)) and related to the perovskite layer.

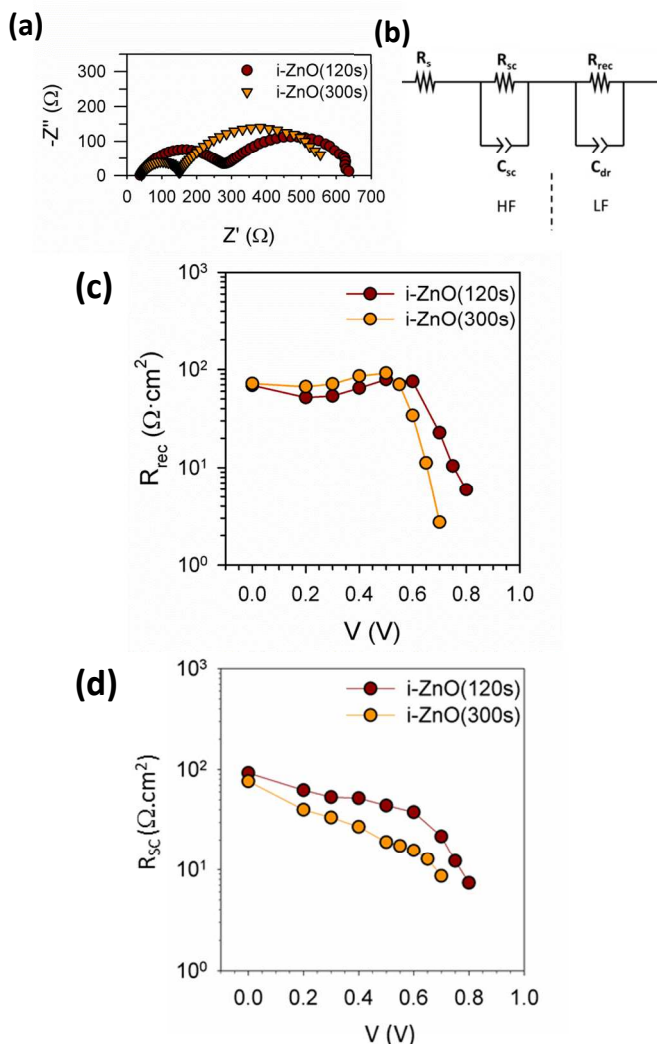


Fig. 6 (a) Nyquist plot under illumination at 0.5V applied bias. (b) Equivalent circuit employed for fitting the impedance spectra (HF: high frequency; LF: low frequency). (c) Recombination resistance, R_{rec} , and (d) selective contact resistance, R_{sc} , under illumination at different applied bias, V.

Very similar R_s , C_{sc} and C_{dr} have been obtained for both samples (see Fig.S5, Supplementary Information). However, significant information can be obtained from R_{sc} and R_{rec} analysis. Fig.6c shows the R_{rec} for both cells. At low applied voltages similar values are obtained but at high applied bias, i-ZnO(120s) presents the highest recombination resistance (the

lowest recombination rate). Consequently, higher V_{oc} observed for i-ZnO(120s) in comparison with i-ZnO(300s) can be unambiguously explained as a result of the lower recombination.⁴⁰ Moreover, higher R_{sc} has been also obtained for i-ZnO(120s) sample (Fig.6d). As HTL material and its deposition process are analogous for both samples, the differences observed can be attributed to the differences introduced by the ETL. The influence of ETL in R_{sc} is associated to two factors. On the one hand, by the transport resistance of electrons through the ZnO ETL. Due to the rather good conductivity of ZnO layers, this resistance can be considered low even for the thicker ZnO layer (sample i-ZnO(300s)). Consequently, we can suppose that R_{sc} is mainly governed by the charge transfer resistance at ZnO-perovskite interface, decreasing as the roughness of the interface increases. This fact can explain the slightly lower FF of this sample in comparison with i-ZnO(300s) sample, as this resistance contributes to the total series resistance (Table 2). The described i-ZnO deposition technique is performed under soft conditions and low temperature. Therefore, it is compatible with lightweight plastic substrates. We have successfully deposited this ETL on PET/ITO sheets and we have prepared flexible solar cells as shown in Fig.S6 (Supplementary Information). The efficiency is low compared to those on ITO/glass (Fig.S6) and would need optimization, however, the prepared cells clearly establish the proof of concept that electrodeposition is a relevant technique for the preparation of ETM for flexible PSC.

Conclusions

We report here the development of a simple and fast deposition method of ETL at low temperature. The progressive nucleation and growth yields to a fully covering film after only two minutes of deposition time. XRD, photoluminescence and Raman spectroscopy analyses have shown that the covering layers are made of high quality ZnO. Moreover the technique can be implemented on ITO-coated flexible plastic substrates. An optimized deposition time of 2 minutes has been defined for their application as ETL in perovskite solar cell. For longer deposition time, the efficiency decreases due to slightly J_{sc} and a V_{oc} reductions. Impedance spectroscopy investigation has shown that the charge transfer resistance between perovskite and ZnO ETL depends strongly on the roughness of the ZnO layer, decreasing as this parameter increases. On the other hand the ZnO ETL also influences the recombination rate. The optimum conditions with an adequate balance of these factors have been determined for PSC with close to 11% efficiency, prepared completely under low temperature conditions. The present work could have important implications in the implementation of low cost industrial processes.

Acknowledgements

J.Z. acknowledges the Guangzhou Government for scholarship (Oversea Study Program of the Guangzhou Elite Project). We thank Dr.Odile Majerus for the help in Raman spectroscopy measurements.

Notes and references

^a Institut de Recherche de Chimie-Paris (IRCP), CNRS-Chimie ParisTech-Paris Sciences et Lettres UMR8247, 11 rue Pierre et Marie Curie, 75005 Paris, France.* Author for the correspondance : thierry.pauporte@chimie-paristech.fr

^b University Jaume I, Department of Physics, Photovoltaic and Optoelectronic Devices Group, Castellon de La Plana 12071, Spain.

Electronic Supplementary Information (ESI) available: SEM view of i-ZnO deposit at short deposition time, Raman and photoluminescence spectra of the i-ZnO layers, bandgap determination and photoluminescence of the CH₃NH₃PbI₃ layer, IPCE curves, R_s and capacitance cell parameters at various voltages and flexible cell characteristics. See DOI: 10.1039/b000000x/

- 1 M. Grätzel, R.A. Janssen, D.B. Mitzi and E.H. Sargent, *Nature*, 2012, **488**, 304.
- 2 R. Plass, S. Pelet, J. Krueger, M. Grätzel and U. Bach, *J. Phys. Chem. B*, 2002, **106**, 7578.
- 3 C. Goh, S.R. Scully and M.D. McGehee, *J. Appl. Phys.*, 2007, **101**, 114503
- 4 H.S. Kim, C.R. Lee, J.H. Im, K.H. Lee, T. Moehl, A. Marchioro, S.J. Moon, R. Humphry-Baker, J.E. Moser and M. Grätzel, *Sci. Rep.*, 2012, **2**, 591.
- 5 M.M. Lee, J. Teuscher, T. Miyasaka, T.N. Murakami and H.J. Snaith, *Science*, 2012, **338**, 643.
- 6 J. Burschka, N. Pellet, S.J. Moon, R. Humphry-Baker, P. Gao, M.K. Nazeeruddin and M. Grätzel, *Nature*, 2013, **499**, 316.
- 7 M. Liu, M.B. Johnson and H.J. Snaith, *Nature* 2013, **501**, 395.
- 8 J.H. Heo, S.H. Im, J.H. Noh, T.N. Mandal, C.S. Lim, J.A. Chang, Y.H. Lee, H.J. Kim, A. Sarkar, M.K. Nazeeruddin, M. Grätzel and S.I. Seok, *Nature Photonics*, 2013, **7**, 487.
- 9 J.H. Noh, S.H. Im, J.H. Heo, T.N. Mandal and S.I. Seok, *NanoLett.* 2013, **13** 1764.
- 10 N.J. Jeon, J.H. Noh, Y.C. Kim, W.S. Yang, S. Ryu and S.I. Seok, *Nature Mater.*, 2014, **13**, 897.
- 11 H. Zhou, Q.Chen, G. Li, S. Luo, T.B. Song, H.S. Duan, Z. Hong, J. You, Y. Liu and Y. Yang, *Science*, 2014, **345**, 542.
- 12 F. Hao, C. C. Stoumpos, D.H. Cao, R.P.H. Chang and M.G. Kanatzidis, *Nature Photonics*, 2014, **8**, 489.
- 13 M. Grätzel, *Nature Mater.*, 2014, **13**, 838.
- 14 Research Cell Efficiency Records, NREL http://www.nrel.gov/ncpv/images/efficiency_chart.jpg
- 15 T. Pauporté, E. Jouanno, F. Pellé, B. Viana, P. Aschehoug, *J. Phys. Chem. C.*, 2009, **113**, 10422.
- 16 B. Liu and H.C. Zeng, *J. Am. Chem. Soc.*, 2003, **125**, 4430.
- 17 J. Zhang, P. Barboux and T. Pauporté, *Adv. Energy Mater.*, 2014, **4**, 1400932.
- 18 D. Q. Bi, G. Boschloo, S. Schwarzmuller, L. Yang, E. M. J. Johansson and A. Hagfeldt, *Nanoscale* 2013, **5**, 11686.
- 19 M.H. Kumar, N. Yantara, S. Dharani, M. Grätzel, S. Mhaisalkar, P.P. Boix and N. Mathews, *Chem. Commun.* 2013, **49**, 11089.
- 20 E.J. Juarez-Perez, M. Wussler, F. Fabregat-Santiago, K. Lakus-Wollny, E. Mankel, T. Mayer and W. Jaegermann, *J. Phys. Chem. Lett.*, 2014, **5**, 680.
- 21 D. Liu and T.L. Kelly, *Nature Photonics*, 2014, **8**, 133.
- 22 K. Mahmood, B.S. Swain and H.S. Jung, *Nanoscale*, 2014, **6**, 9127.
- 23 D.Y. Son, J.H. Im, H.S. Kim and N.G. Park *J. Phys. Chem. C*, 2014, **118**, 16567.
- 24 J. Dong, Y. Zhao, J. Shi, H. Wei, J. Xiao, X. Xu, J. Luo, J. Xu, Y. Li, Y. Luo and Q. Meng, *Chem. Comm.*, 2014, **50**, 13381.
- 25 C. Magne, T. Moehl, M. Urien, M. Grätzel and T. Pauporté, *J. Mater. Chem.A*, 2013, **1**, 2079.
- 26 M. Law, L.E. Greene, J.C. Johnson, R. Saykally and P.D. Yang, *Nature Mater.*, 2005, **4**, 455.
- 27 V.M. Guérin and Th. Pauporté, *Energy Environ. Sci.*, 2011, **4**, 2971-2979.
- 28 M. Izaki and T. Omi, *Appl. Phys. Lett.*, 1996, **68**, 2439.
- 29 M. Izaki and T. Omi, *J. Electrochem. Soc.*, 1996, **143**, L53.
- 30 T. Shinagawa, M. Chigane, K. Murase and M. Izaki, *J. Phys. Chem. C*, 2012, **116**, 15925.
- 31 M. Izaki, T. Ohta, M. Kondo, T. Takahashi, M. Fariza, J. Sasano, T. Shinagawa and T. Pauporté, *ACS Appl. Mater. Interf.*, 2014, **6**, 13461.
- 32 L. Etgar, O. Gao, Z. Xue, Q. Pen, A.K. Chandiran, B. Liu, M.K. Nazeeruddin and M. Grätzel, *J. Am. Chem. Soc.*, 2012, **134**, 17396.
- 33 T. Pauporté and I. Jirka, *Electrochim. Acta.*, 2009, **54**, 7558.
- 34 Powder Diffraction File card 36-1451, Joint Committee on Powder Diffraction Standards, ICDD, Newtown Square (PA) 2001.
- 35 O. Lupan, T. Pauporté, L. Chow, B. Viana, F. Pellé, B. Roldan Cuenya, L.K. Ono and H. Heinrich, *Appl. Surf. Sci.*, 2010, **256**, 1895.
- 36 R. Cusco, E. Alarcon-Llado, J. Ibanez and L. Artus, *Phys. Rev. B*, 2007, **75**, 165202.
- 37 O. Lupan, L. Chow, L.K. Ono, B. Roldan Cuenya, G. Chai, H. Khallaf, S. Park and A. Schulte, *J. Phys. Chem. C*, 2010, **114**, 12401.
- 38 H.J. Snaith, A. Abate, J. Ball, G.E. Eperon, T. Leijtens, N.K. Noel, S.D. Stranks, T.J.W. Wang, K. Wojciechowski, W. Zhang, *J. Phys. Chem. Lett.* 2014, **5**, 1511.
- 39 J. Bisquert, L. Bertoluzzi, I. Mora-Sero and G. Garcia-Belmonte, *J. Chem. Phys. C*, 2014, **118**, 18983.
- 40 B. Suarez, V. Gonzalez-Pedro, T.S. Ripolles, R.S. Sanchez, L. Otero and I. Mora-Sero, *J. Chem. Phys. Lett.* 2014, **5**, 1628.

Graphical and textual abstract

A fast, simple and low temperature growth technique is described for the preparation of high structural and optical quality ZnO layers. These layers are shown to act as efficient selective contacts in perovskite solar cell.

